# Salt shape tomography

*Patrice Guillaume*, Stanislaw Warzocha, Olivier Hermant and Anthony Prescott, CGG*

**Summary**

In subsalt imaging salt bodies are usually delineated using scenario-based migration scans. Estimating the shape of salt bodies remains a challenge. Assuming that variations of velocity in salt are small, we have developed an original tomography method for estimating the shape of salt bodies. The data to invert mainly consist of residual moveout (RMO) observed below salt bodies on migrated common image point gathers (CIGs). Using ray-based nonlinear slope tomography we compute Fréchet derivatives made of traveltime derivatives with respect to depth parameters describing salt bounding surface to re-position. Salt shape is progressively updated after each linearized tomographic step. We demonstrate the method on a 2D synthetic example and on a high-fold 3D land dataset from the Sultanate of Oman.

**Introduction**

Velocity model building using migration velocity analysis (Al-Yahya, 1989; Woodward et al., 1998) aims at computing an accurate velocity model for seismic imaging and interpretation purposes. When applied to surface seismic data we have to solve an underdetermined and ill-posed inverse problem that requires relevant constraints and benefits from a nonlinear approach involving iterative linearized updates (Guillaume et al., 2001). In linear gridded tomography (Woodward et al., 1998), velocity model parameters consist of regular 3D grids describing continuous spatial variations of velocity and/or anisotropy.

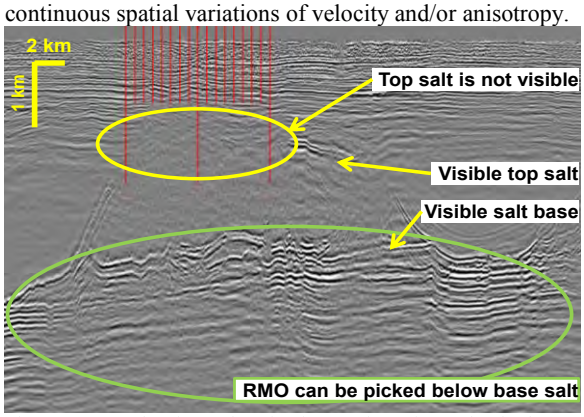


Figure 1: Depth-migrated seismic section from land dataset showing a salt body. The top salt boundary is not visible in the yellow circle. Orange arrows show visible parts of top and base salt boundaries. RMO can be picked in green circled subsalt area.

The gridded approach cannot easily handle strong velocity contrasts that can exist between different geological units (chalk, salt…) unless adaptive meshing is used.

Solutions for handling horizons and velocity contrasts have been proposed in the past (Delprat-Jannaud and Lailly, 1993; Sinoquet, 1993; Guiziou et al., 1996) for inverting horizon-related traveltime information. More recently, multi-layer tomography (Guillaume et al, 2012) inverting RMO picked in a volumetric sense made it possible both to compute continuous spatial variations of velocity simultaneously inside several layers and to reposition the layer boundaries corresponding to major velocity contrasts, thus avoiding drawbacks of layer stripping approach which accumulates errors with depth. Velocity perturbations are the unknowns of a linear system to solve, and layer boundaries are modelled again using updated velocities. Multi-layer tomography techniques assume the layer boundaries can be picked on an initial migrated seismic image for deriving model independent repositioning quantities (including traveltime and traveltime slopes). However, situations exist where interfaces characterized by strong velocity contrasts cannot be picked everywhere. This occurs frequently in salt context, as shown by the migrated vertical section in Figure 1. This figure illustrates the situation we want to address, where:

- Top or base layer boundary is partly not visible (e.g. in case of weak impedance contrast). Traveltime information required for map-migrating the boundaries cannot be obtained, thus preventing from updating layer shape within multi-layer tomography workflow.
- Intra-layer variations of velocity are weak and/or have less impact on traveltimes than the changes in the layer shape.
- Intra-layer reflectors are rare, thus preventing from picking RMO inside the layer.
- RMO can be picked below the layer of interest.

We propose to invert sub-layer RMO information in order to estimate the position of parts of top or base layer boundary where not visible: in those parts of the model, layer shape is updated rather than the spatial variations of velocity inside the layer of interest. The proposed method is an extension of the multi-layer tomography which complements the nonlinear slope tomography toolbox. After a brief introduction to nonlinear slope tomography, we present the new tomographic equations. We demonstrate the method on a simple synthetic example and then apply it to a high fold land field dataset.

**Nonlinear slope tomography**

Kinematic information in slope tomography consists of a set of model independent quantities called “kinematic invariants” (Guillaume et al., 2001) obtained by kinematical de-migration of locally coherent events picked


DOI http://dx.doi.org/10.1190/segam2015-5818826.1

in the pre-stack migrated time or depth domain. The kinematic invariants are characterized by their shot and receiver positions ***(r, s)*** and by their local traveltime and traveltime slopes in the un-migrated data-cube $(T_{obs}, \partial T_{obs}/\partial m, \partial T_{obs}/\partial h)$, where $m$ denotes the mid-point position and $h$ the vector offset. For a given velocity model these invariants can be kinematically re-migrated in depth. We obtain the position and dip of the associated re-migrated locally coherent events as well as the local derivatives with respect to offset of the RMO curve/surface, *dRMO* (Chauris et al., 2002). Nonlinear slope tomography described by Montel et al. (2010, 2011) aims at minimizing *dRMO* through a nonlinear local optimization of the velocity.

**Method**

During one given linearized step of the nonlinear workflow and following the slope tomography equations of Chauris et al. (2002), the linear system to solve is built from the Fréchet derivatives which relate *dRMO* slope variations to perturbations of velocity model parameters. Here the selected depth and velocity parameters to estimate should not be coupled to avoid adding ambiguity to ill-posed tomographic problem. In the simplest implementation, velocity or anisotropy parameters can be replaced by depth parameters $Z(x, y)$ describing the invisible part of the layer boundary to update: $\partial dRMO/\partial V(x, y, z)$ is replaced by $\partial dRMO/\partial Z(x, y)$. Both derivatives can be expressed in terms of traveltime derivatives through same relation $f$:

$$\partial dRMO/\partial V(x, y, z) = f(\partial T/\partial V(x, y, z)) \quad (1)$$

$$\partial dRMO/\partial Z(x, y) = f(\partial T/\partial Z(x, y)) \quad (2)$$

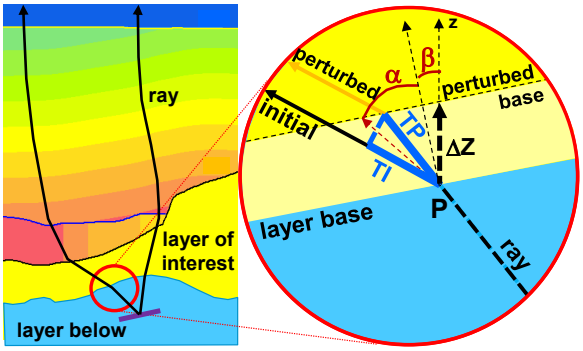


Figure 2: Ray and traveltime perturbations associated to local ΔZ depth perturbation of layer base boundary at position P

Geometrical interpretation of traveltime derivative with respect to depth parameter for ray-path hitting layer base boundary at position P is given in Figure 2: a shift upward of layer boundary altitude by ΔZ will change ray traveltime by $(TP- TI)$. Traveltime derivative can be written as

$$\partial T/\partial Z(x, y) \approx (U_{g\text{-}b}(P) - U_g(P))\cos\beta/\cos\alpha \quad (3)$$

Where $U_{g\text{-}b}(P)$ is group velocity below layer base boundary, $U_g(P)$ is group velocity in layer of interest, β is structural dip angle of layer boundary and α is approximately the average ray incidence angle.

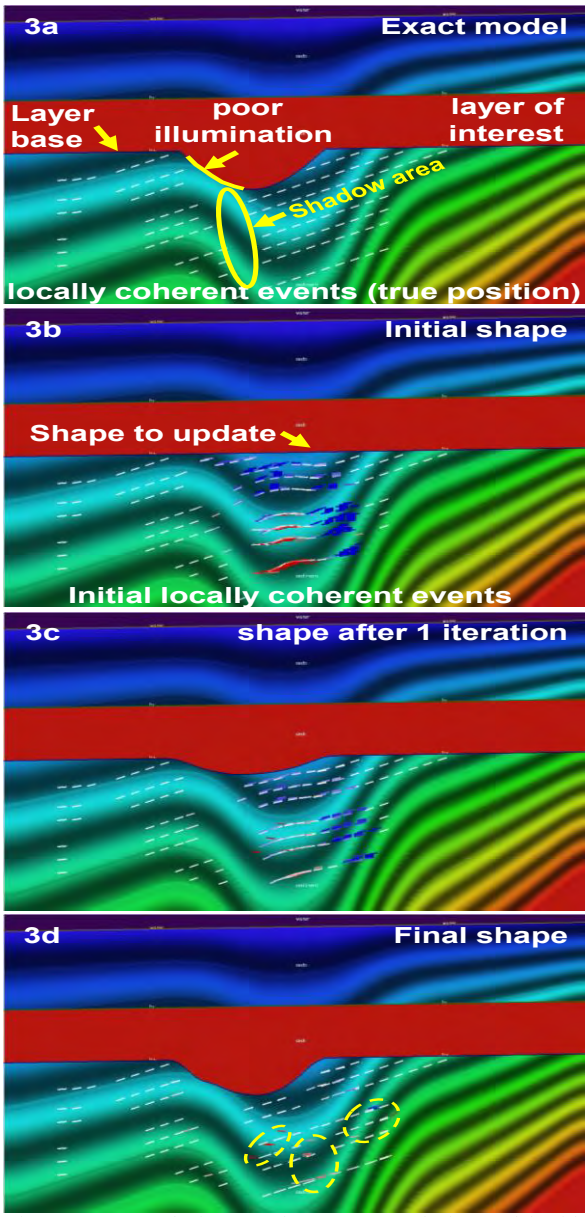


Figure 3: 2D Synthetic example. (a) Exact velocity model with exact shape of red layer of interest. The poorly illuminated part of layer base boundary is highlighted in yellow and corresponding shadow area below it is circled in yellow. (b) Initial model with correct velocities but no syncline in red layer. Color code for representing migrated locally coherent events: blue=RMO curving up, red=RMO curving down, white=no RMO. (c) After one internal tomography iteration the syncline starts to appear. (d) Final shape of syncline after 8 internal tomography iterations. Possible multi-arrivals are circled in yellow.


DOI http://dx.doi.org/10.1190/segam2015-5818826.1

**2D synthetic example**

The 2D TTI synthetic model shown in Figure 3 contains a salt velocity layer with a local syncline with dips up to 45 degrees and a series of plane dipping (19 degrees) subsalt reflectors used for RMO picking. Part of the syncline is not illuminated by the RMO data, a common situation encountered with field datasets. The initial model (Figure 5b) has correct velocities but no syncline structure. Locally coherent events below the missing syncline structure are neither correctly focused nor correctly positioned. Note the distorted reflectors and associated RMO. Figures 3c and 3d show how the syncline gets progressively updated respectively after one and eight internal tomography iterations. After 8 nonlinear iterations (final model) the subsalt reflectors become planar with correct dip and position, and the RMO gets minimized. The salt shape update is guided by regularization terms in the poorly illuminated parts of the syncline. In the final updated model, most re-migrated locally coherent events are at the correct position and aligned whatever the offset value, the final RMO is almost null (white) and the shape of the layer boundary is satisfactory, where illuminated. Some events have migrated to wrong positions with strong remaining RMO. This suggests that multi-pathing associated with our common offset migration may have occurred due to boundary geometry and that careful handling of those exceptions is required. Changes in salt shape between first and last iteration illustrate the non-linearity of the problem to solve.

**3D high-fold land dataset from the Sultanate of Oman**

Figure 4a shows a migrated section exhibiting a salt body in depth range 2000-3500m and a subsalt area made of gently dipping reflectors. The geological setting in this area is such that the top salt boundary is partly invisible due to the lack of impedance contrast at top salt combined with the presence of multiples obscuring the faint top salt reflector. As a consequence, and despite using multi-layer tomography with four azimuth sectors, the top salt interpretation and hence the velocity model are inaccurate in some places. Moreover, subsalt reflectors are distorted and not well focused as shown in Figure 4b by the CIGs for the Azimuth 0 sector at positions corresponding to red comb in Figure 4a.

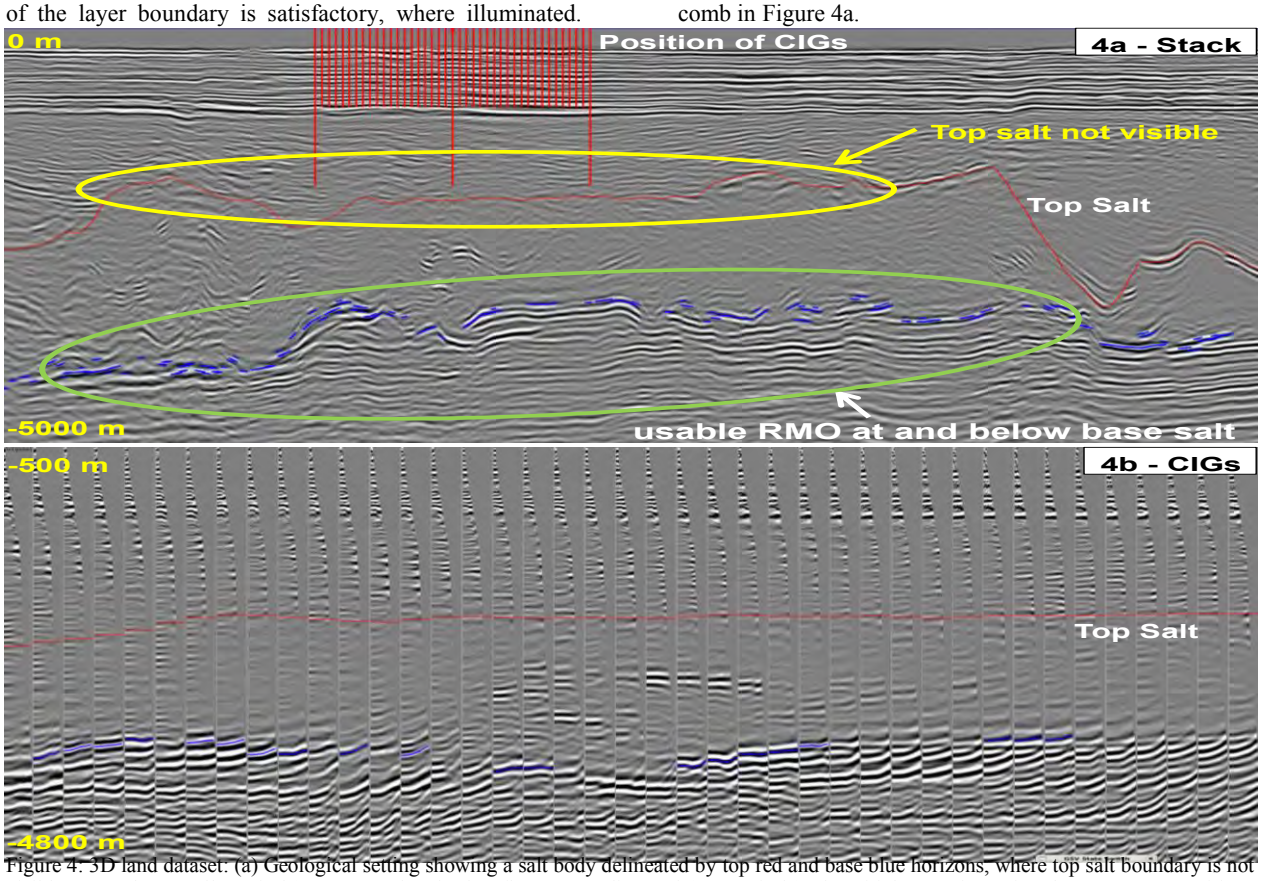


Figure 4: 3D land dataset: (a) Geological setting showing a salt body delineated by top red and base blue horizons, where top salt boundary is not visible everywhere (yellow circle). As a result subsalt reflectors are distorted (green circle). (b) Initial CIGs for Azimuth 0° sector at positions corresponding to red comb in (a). RMO curving up can be observed in subsalt part below blue horizon.


DOI http://dx.doi.org/10.1190/segam2015-5818826.1

RMO curving up can be observed in subsalt part. Starting with the initial model shown in Figure 5a, the salt shape tomography is applied to update the top salt shape only: the updated model in Figure 5e and resulting image in Figure 5f can be compared with the initial model and seismic (Figures 5a, 5b) and with the result obtained after a manual update of top salt (Figures 5c, 5d). Overall, subsalt reflectors imaged after salt shape tomography are less distorted, more continuous and better focused, as shown by the red arrows in Figure 5f.

## Conclusions

We have presented a method for estimating the shape of either top or base boundary of salt layer (or any other geological feature) by inverting sub-salt RMO using nonlinear slope tomography. The synthetic example has shown that the progressive and quite nonlinear update of salt shape reaches a satisfactory result. RMO for most imaged events is correctly minimized, but some exceptions suggest that multi-pathing may occur and that careful handling of those exceptions is required. The application of the method to a 3D land dataset where top salt boundary is not visible in many areas gives encouraging results: the nonlinear inversion of subsalt RMO results in more continuous, less distorted and better focused reflectors in subsalt image. The Salt shape tomography result is better in the subsalt area compared to a manual salt scenario-based result. This method can thus help the geophysicist reduce the number of scenarios to test.

## Acknowledgments

We wish to thank the Ministry of Oil and Gas of the Sultanate of Oman and Petroleum Development Oman for permission to publish this paper.

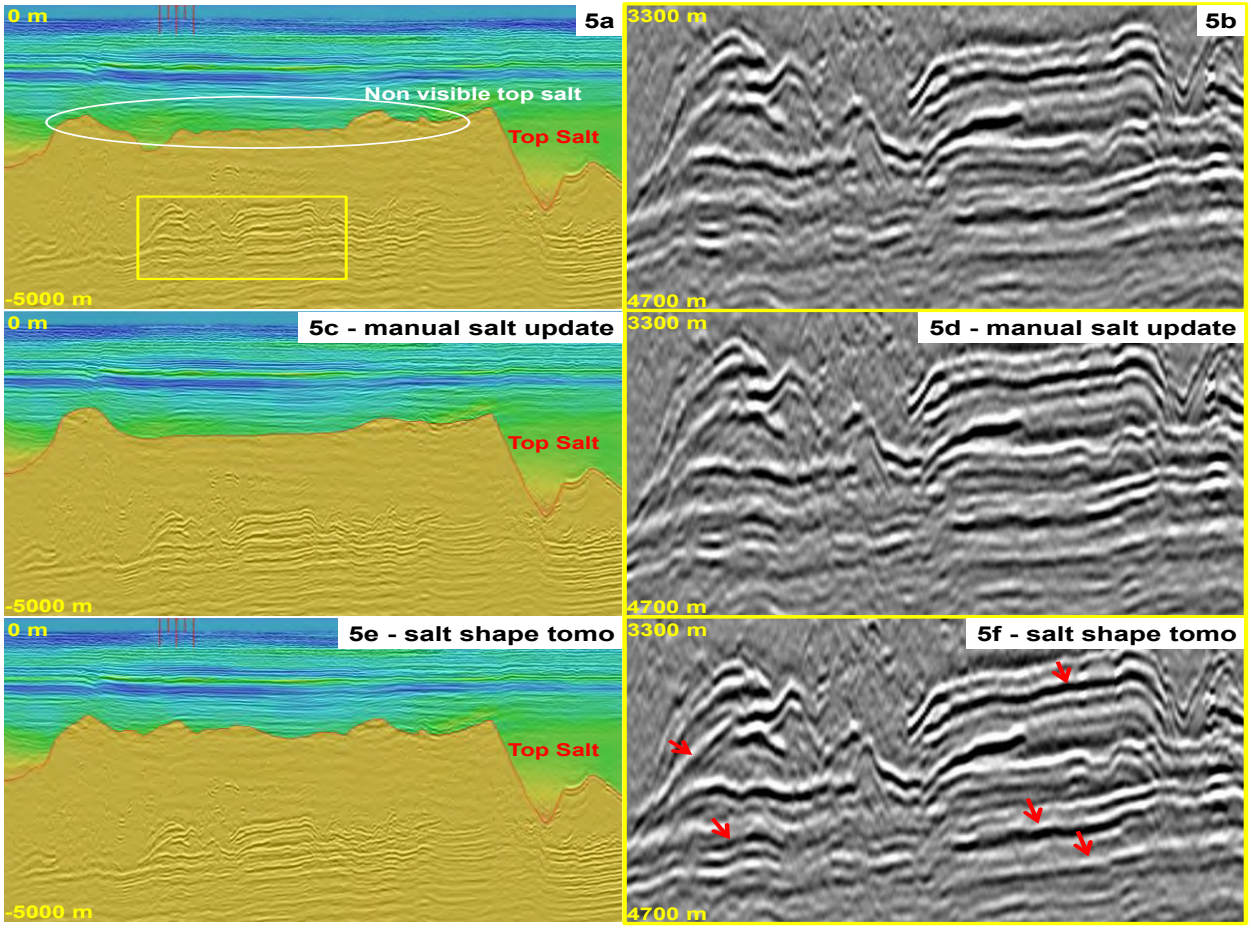


Figure 5: 3D land dataset: (a) Initial model after conventional tomography: velocity model with initial top salt shape. (b) Resulting seismic image corresponding to the yellow rectangle sketched in (a). (c) Updated velocity model with manually-set top salt shape. (d) Resulting seismic image. (e) Top salt shape updated by salt shape tomography. (f) Resulting seismic image: the red arrows highlight more realistic and more continuous reflectors. Seismic images in (b), (d) and (f) correspond to the yellow rectangle sketched in (a).


DOI http://dx.doi.org/10.1190/segam2015-5818826.1

**EDITED REFERENCES**

Note: This reference list is a copyedited version of the reference list submitted by the author. Reference lists for the 2015 SEG Technical Program Expanded Abstracts have been copyedited so that references provided with the online metadata for each paper will achieve a high degree of linking to cited sources that appear on the Web.

**REFERENCES**


Al-Yahya, K. M., 1989, Velocity analysis by iterative profile migration: Geophysics, **54**, 718–729, http://dx.doi.org/10.1190/1.1442699.

Chauris, H., M. S. Noble, G. Lambaré, and P. Podvin, 2002, Migration velocity analysis from locally coherent events in 2-D laterally heterogeneous media, Part I: Theoretical aspects: Geophysics, **67**, no. 4, 1202–1212, http://dx.doi.org/10.1190/1.1500383.

Delprat-Jannaud, F., and P. Lailly, 1993, Ill-posed and well-posed formulations of the reflection travel time tomography problem: Journal of Geophysical Research, **98**, B4, 6589–6605, http://dx.doi.org/10.1029/92JB02441.

Guillaume, P., F. Audebert, P. Berthet, B. David, A. Herrenschmidt, and X. Zhang, 2001, 3D Finite-offset tomographic inversion of CRP-scan data, with or without anisotropy: 71st Annual International Meeting, SEG Expanded Abstracts, 718–721.

Guillaume, P., S. Hollingworth, X. Zhang, A. Prescott, R. Jupp, G. Lambaré, and O. Pape, 2012, Multi-layer tomography and its application for improved depth imaging: 82nd Annual International Meeting, SEG, Expanded Abstracts, http://dx.doi.org/10.1190/segam2012-0683.1.

Guiziou, J.-L., J.-L. Mallet, and R. Madariaga, 1996, 3D seismic reflection tomography on top of the GOCAD depth modeler: Geophysics, **61**, 1499–1510, http://dx.doi.org/10.1190/1.1444075.

Montel, J.-P., P. Guillaume, G. Lambaré, and O. Leblanc, 2010, Non-linear slope tomography — Extension to MAZ and WAZ: 72nd Conference & Exhibition, EAGE, Extended Abstracts, 4431–4435, doi:10.3997/2214-4609.201401159.

Montel, J.-P., G. Lambaré, and P. Guillaume, 2011, Non-linear slope tomography from RTM and Kirchhoff angle domain common-image gathers: 71st Annual International Meeting, SEG, Expanded Abstracts, 3984–3988.

Sinoquet, D., 1993, Modeling a priori information on the velocity field in reflection tomography: 63rd Annual International Meeting, SEG, Expanded Abstracts, 592–595.

Woodward, M., P. Farmer, D. Nichols, and S. Charles, 1998, Automated 3D tomographic velocity analysis of residual moveout in prestack depth migrated common image point gathers: 68th Annual International Meeting, SEG, Expanded Abstracts, 1218–1221, doi: 10.1190/1.1820113.



DOI http://dx.doi.org/10.1190/segam2015-5818826.1